Rare Metal Materials and Engineering
Volume 55, Issue 1, January 2026
Available online at www.rmme.ac.cn

Science Press

Cite this article as: Li Yaguan, Nie Zhenguo, Li Huilin, et al. Intelligent Parameter Decision-Making and Multi-objective Prediction for Multi-layer and Multi-pass LDED Process[J]. Rare Metal Materials and Engineering, 2026, 55(01): 47-58. DOI: https://doi.org/10.12442/j.issn.1002-185X.20250065.

ARTICLE

Intelligent Parameter Decision-Making and Multi-objective Prediction for Multi-layer and Multi-pass LDED Process

Li Yaguan[1,2], Nie Zhenguo[2,3,4], Li Huilin[2], Wang Tao[1], Huang Qingxue[1]

[1] College of Mechanical Engineering, Taiyuan University of Technology, Taiyuan 030024, China; [2] Department of Mechanical Engineering, Tsinghua University, Beijing 100084, China; [3] State Key Laboratory of Tribology in Advanced Equipment, Tsinghua University, Beijing 100084, China; [4] Beijing Key Laboratory of Precision/Ultra-precision Manufacturing Equipment and Control, Tsinghua University, Beijing 100084, China

Abstract: The key parameters that characterize the morphological quality of multi-layer and multi-pass metal laser deposited parts are the surface roughness and the error between the actual printing height and the theoretical model height. The Taguchi method was employed to establish the correlations between process parameter combinations and multi-objective characterization of metal deposition morphology (height error and roughness). Results show that using the signal-to-noise ratio and grey relational analysis, the optimal parameter combination for multi-layer and multi-pass deposition is determined as follows: laser power of 800 W, powder feeding rate of 0.3 r/min, step distance of 1.6 mm, and scanning speed of 20 mm/s. Subsequently, a Genetic Bayesian-back propagation (GB-BP) network is constructed to predict multi-objective responses. Compared with the traditional back propagation network, the GB-back propagation network improves the prediction accuracy of height error and surface roughness by 43.14% and 71.43%, respectively. This network can accurately predict the multi-objective characterization of morphological quality of multi-layer and multi-pass metal deposited parts.

Key words: multi-layer and multi-pass laser cladding; Taguchi method; grey relational analysis; GB-BP network

1 Introduction

Laser-directed energy deposition (LDED) is a specific additive manufacturing technique that employs precise process parameters to produce solid workpieces. It enables surface modification of workpieces through a specialized cladding layer, enhancing their resistance to high-temperature wear and corrosion. Due to its inherent characteristics, such as high energy density, high efficiency, high design freedom, rapid fabrication speed, and exceptional physical and mechanical properties, LDED is extensively applied in aerospace[1], medical equipment[2], and the manufacturing of other large-sized components[3]. Metal powder is the commonly used raw material in this process, in which a nozzle injects the powder into the molten pool under the action of a carrier gas, which then cools and solidifies.

With the rapid development of laser cladding technology[4], there has been an increasing demand for higher surface forming quality of workpieces, while the tolerance for shape and size deviations in multi-layer and multi-pass cladding processes has become more stringent.

The laser cladding process involves various parameters, including laser spot diameter, laser power, powder-feeding rate, scanning speed, overlap rate, shielding gas flow rate, and powder-feeding gas flow rate. Different parameter combinations affect the forming quality of the cladded parts[5–7]. Extensive research has been conducted on the influence of single-layer cladding processes on cladding height, width, and depth[8], as well as the influence of process design on properties such as strength, hardness, high-temperature resistance, and corrosion resistance of the cladding layer[9–11]. Numerous experimental verifications have been employed to analyze how different process parameters affect the single-layer cladding[12]. The Taguchi method, response surface methodology, and grey relational analysis are commonly used for parameter optimization and response

Received date: February 10, 2025
Foundation item: National Natural Science Foundation of China (52175237)
Corresponding author: Nie Zhenguo, Ph. D., Professor, Department of Mechanical Engineering, Tsinghua University, Beijing 100084, P. R. China, E-mail: zhenguonie@tsinghua.edu.cn

prediction[13–14]. Marzban et al[15] conducted orthogonal experiments and found the optimal solution by combining principal component analysis with the technique for order preference by similarity to ideal solution. Deng et al[16] combined the Taguchi method with grey relational analysis to optimize the multi-objective response parameters of TiC particle-reinforced iron-based composite cladding layers prepared by preset powder laser cladding. Mondal et al[17] conducted orthogonal experiments to study the effects of laser power, scanning speed, and powder-feeding rate on cladding layer quality on AISI1040 steel substrates, and proposed a multi-objective response approach using grey relational analysis to determine optimal process parameters. Quazi et al[18] adopted the Taguchi optimization method and used signal-to-noise ratio (SNR) response analysis and Pareto analysis of variance to analyze results. Experimental validation of the optimized parameter combination revealed significant improvements in surface hardness and roughness of the AA5083 cladding layer. Yu et al[19] used the Taguchi grey relational method to optimize the process parameters for laser cladding of Fe313, with cladding width, height, and dilution rate selected as response targets. Their findings demonstrated that the optimized cladding layer exhibits improved morphology and structure compared to the unoptimized layer. Lian et al[20] designed a Taguchi experiment to study the effects of process parameters on the microhardness and wear volume of the cladding layer, aiming to improve its performance. The grey relational analysis method was used to determine the optimal process parameters and predict their grey relational grade (GRG). The results showed that the average error between the predicted and experimental results was 5.3%. Lee et al[21] investigated the impact of process parameters on the geometry of single-pass laser cladding layers of AISI M4 and employed response surface methodology to establish a mathematical model for predicting and controlling the layer geometry. Alam et al[22] employed the central composite response surface methodology to design orthogonal experiments, focusing on the influence of selected process parameters on the geometry and hardness of single-pass laser cladding layers of AISI 420 metal powder. A multivariate regression model was also established to predict the hardness of cladding layer, the aspect ratio of weld bead, and the wetting angle of substrate. Bhardwaj et al[23] studied the influence of process parameters (laser power, scanning speed, and powder feeding rate) on the geometric properties of cladding layers, especially the dilution rate, based on the response surface method and variance analysis. The mapping relationship between parameters and geometric properties was established by regression modeling to find the optimal experimental parameters.

In addition to the aforementioned traditional methods, machine learning and artificial neural networks, especially back propagation (BP) neural networks, have been widely used in laser cladding for process parameter optimization and multi-objective response prediction[24–25]. Li et al[26] developed a BP neural network to predict the influence of process parameters on dilution rate, and its prediction error was 5.89%. However, this model is highly dependent on the dataset size and tends to fall into local minima when the number of samples is restricted. Swarm intelligence algorithm, such as genetic algorithm (GA) [27], have strong global optimization capabilities. Therefore, many scholars have proposed combining GA with BP networks to solve problems such as slow GA convergence and susceptibility to local minima, thereby achieving fast and accurate global optimization. Ilanlou et al[28] performed a full factorial experiment to investigate the influence of process parameters on the geometric characteristics of Inconel 718 rails. They predicted the geometric characteristics of the cladding layer through linear regression and GA under different parameter combinations. Yang et al[29] integrated BP neural networks with GA to establish a prediction model that links process parameters to the surface morphology quality of laser cladding layers, and verified the prediction accuracy of the model through experiments. Liu et al[30] established a GA-BP neural network, using laser power, scanning speed, and powder thickness as process parameters. They conducted a full factorial experiment to generate a dataset and predicted the geometric characteristics of single-layer and single-pass cladding layers produced by a high-power semiconductor laser. Yu et al[31] designed an orthogonal experiment with overlap rate, powder feeding rate, and scanning speed as process parameters, and established a neural network model to predict the crack density of high-hardness nickel-based laser cladding layers. The results were optimized using GA, and the reliability of model was validated through experiments. Deng et al[32] designed a Taguchi experiment and used the SNR and variance analysis method to analyze the effects of laser power, spot diameter, overlap rate, and scanning speed on the micro-hardness of Ti(C, N) ceramic cladding layers. Furthermore, a BP neural network combined with a quantum particle swarm optimization algorithm was employed to establish a mapping relationship between process parameters and responses for accurate prediction. Wang et al[33] developed a powder-scale multi-physics model, which incorporated mass transfer, phase change, and heat transfer during the LDED process to predict the geometric characteristics of single-layer and single-pass cladding tracks. In addition, a Gaussian regression model was also established to predict the geometry of cladding tracks under various parameter combinations.

Existing parameter optimization methods for LDED primarily focus on single-layer single-pass or single-layer multi-pass cladding, with few research on multi-layer and multi-pass cladding. However, due to the heat accumulation between layers, the manufacturing accuracy of multi-layer and multi-pass cladding is more sensitive to process parameters. Furthermore, when orthogonal tests involve many factors, it is difficult to determine the variation pattern in the experimental data. The optimal result is usually a combination of parameters, which can not only accurately predict the height error and surface roughness but also obtain the optimal process parameters.

In this study, the Taguchi method was used to design orthogonal experiments, and the SNR of multi-objective responses was analyzed. Additionally, the grey relational analysis method was used to predict the optimal parameters for multi-layer and multi-pass cladding, aiming to minimize both the theoretical and actual height error (ΔH) of the printed parts and the surface roughness (R_a). Experimental verification was then conducted. Subsequently, a GB-BP network was constructed to predict multi-objective responses.

2 Experiment

Fig.1 illustrates the research approach, which includes laser cladding equipment and a visual inspection system. Point cloud data were collected to calculate the height difference and surface roughness of the printed parts. A hybrid approach employing the Taguchi method and grey relational analysis was used to identify the optimal parameter combination. Furthermore, a GB-BP network model was constructed for multi-objective response prediction.

2.1 Materials and equipment

The printing equipment includes an optical platform, a three-axis motion system, a control console, a powder feeder, a laser, a powder feeder barrel, a water cooler, and a structured light camera. The structured light camera projects a custom-designed pattern onto the surface of the three-dimensional object while utilizing an integrated camera to capture the image distortion on the physical surface.

The substrate used in the experiment was 316 stainless steel with dimensions of 100 mm×100 mm×8 mm. The experiments used gas-atomized 316L powder (Carpenter Additive) with a particle size of 53 – 120 μm. 316L powder was mainly spherical, with fine satellite particles adhering to the surface of powder particles. The composition of both the powder and the substrate was confirmed using energy dispersive spectrometer (EDS), and their elemental composition is presented in Table 1. Before laser cladding, the metal powders were incubated in a drying oven at 100 ℃ for 2 h. The dried powder was then loaded into the powder hopper, ready for deposition onto the substrate via the laser cladding process. Before deposition, the substrate surface was cleaned with anhydrous ethanol to remove contaminants. After drying, the experiment was conducted.

The experiment used a laser cladding system with a maximum output power of 2000 W. The laser spot diameter was 2 mm, and high-purity argon was used as the shielding gas and powder-feeding gas during cladding. After multi-layer laser cladding, a 3D point cloud model of the component was acquired using an optical camera to calculate its ΔH and R_a. Under ideal conditions, the surface coating formed by multi-pass cladding exhibited a cross-section with relatively regular convex and concave morphologies. Fig.2 illustrates the profile curve of this cross-section, and the roughness R_a can be calculated by Eq.(1).

$$R_a = \frac{\int_0^L |z(x)|\,dx}{L} = \frac{1}{n}\sum_{i=1}^{n}|z_i| \quad (1)$$

where $z(x)$ is the longitudinal distance of the section profile; L is the transverse distance of the section contour; n is the number of test points; z_i is the longitudinal distance of the cross-section profile of each test point.

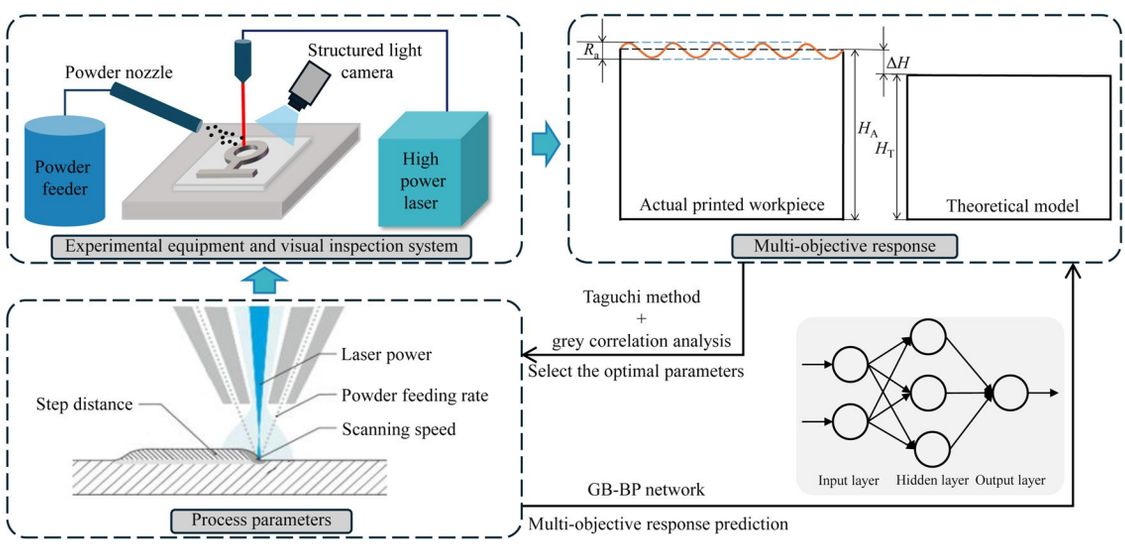

Fig.1 Schematic diagram and flowchart of laser cladding system

The multi-layer and multi-pass laser deposition process gradually achieved the preparation or repair of complex structures by the gradual deposition of metal materials in multiple layers (via repeated superposition) and multiple passes (each pass follows a different direction). In this process, the laser beam was focused on the metal surface and

Table 1 Composition of substrate and powder materials (wt%)

Element	C	Cr	Si	Ni	Mn	Mo	Fe
Substrate	0.03	17.0	0.5	13.0	0.2	2.0	Bal.
Powder	0.06	18.16	0.49	8.05	1.06	0.11	Bal.

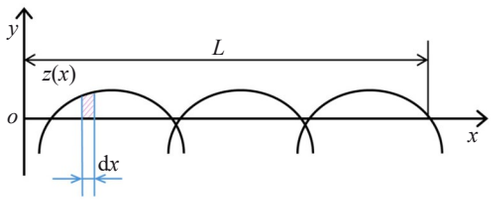

Fig.2 Profile curve of ideal coating cross-section

locally heated it to a molten state. The molten metal combined with the feed powder or wire to form a molten pool. In each layer, the molten pool followed a predetermined scanning trajectory, and once a layer was completed, the deposited molten metal underwent rapid cooling and solidification. The laser was applied continuously on the new layer to form a metallurgical bond with the previous layer. This process was repeated until the target part geometry was achieved. The repeated cross-scanning characteristics of this process imposed higher requirements on the scanning path and direction[34]. The filling path determined the internal structure of the printed model, thereby directly affecting the strength and stability of the prepared object.

The angle setting of linear filling impacts the strength, appearance, and stability of the printed parts in 3D printing. The linear filling angle affects the strength of the printed parts in different directions. Usually, the strength direction of the printed part is parallel to the direction of the filling path. Commonly used filling angles are 0°, 45°, 90°, and 135°, and the filling path at each angle provides different strength support. For instance, parts filled at 0° and 90° perform well under lateral and longitudinal pressures, respectively. Filling angles of 45° and 135° provide balanced support in multiple directions. Due to the staggered layout of 45° and 135° angles, they can share strength in multiple directions, generally yielding more uniform strength compared to horizontal or vertical filling[35]. Therefore, this work adopted the second filling method, as shown in Fig. 3a, and the effect of multi-layer and multi-pass cladding using this method is shown in Fig.3b.

2.2 Experimental design

In this study, laser power, powder feeding rate, step distance, and scanning speed were selected as the key factors influencing the flatness of the top surface of component. Table 2 lists these four factors and their corresponding levels. A $L_{16}(4^4)$ Taguchi orthogonal experimental design was adopted, with the orthogonal array presented in Table 3. Two response items, ΔH and R_a, were selected to evaluate the printing quality, aiming to obtain a multi-layer cladding workpiece with excellent comprehensive performance.

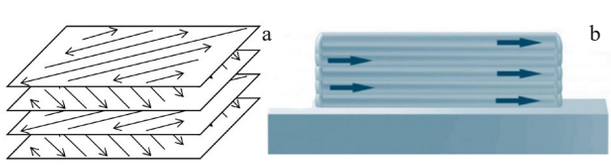

Fig.3 Schematic diagrams of filling path direction (a) and effect of multi-layer and multi-pass cladding (b)

Table 2 Process parameters of laser cladding and corresponding levels

Parameter	Level			
	1	2	3	4
Laser power, LP/W	800	900	1000	1100
Powder feeding rate, PR/r·min^{-1}	0.3	0.4	0.5	0.6
Step distance, SD/mm	1.0	1.2	1.4	1.6
Scanning speed, SS/mm·s^{-1}	16	18	20	22

Table 3 $L_{16}(4^4)$ taguchi orthogonal experimental design

No.	LP/W	PR/r·min^{-1}	SD/mm	SS/mm·s^{-1}
1#	900	0.6	1.0	16
2#	1000	0.4	1.2	16
3#	800	0.6	1.2	20
4#	1100	0.3	1.2	18
5#	800	0.5	1.0	18
6#	900	0.5	1.2	22
7#	1000	0.3	1.0	22
8#	1100	0.4	1.0	20
9#	800	0.3	1.4	16
10#	1000	0.5	1.4	20
11#	1100	0.6	1.4	22
12#	900	0.4	1.4	18
13#	1100	0.5	1.6	16
14#	900	0.3	1.6	20
15#	1000	0.6	1.6	18
16#	800	0.4	1.6	22

3 Results and Discussion

3.1 Experiment results

Different combinations of process parameters will result in different thicknesses of the cladding layer. Therefore, it is imperative to determine the single-layer cladding thickness corresponding to each parameter combination before multi-layer cladding. The 16 sets of parameters in Table 3 were used for laser cladding, and the single-layer cladding height (H_1) was measured as the benchmark thickness for multi-layer cladding.

Fig. 4 illustrates the experimental results of cladding a single layer, and Table 4 provides the thickness of the cladding layer corresponding to different parameters.

The target heights for 16 parameter combinations were used as the baselines, and multi-layer cladding was performed accordingly. The experimental results are shown in Fig.5. Due to the installation constraints of the measuring equipment, the maximum achievable printing height in the current can reach 20 mm. Within this range, it is reasonable to use ΔH to

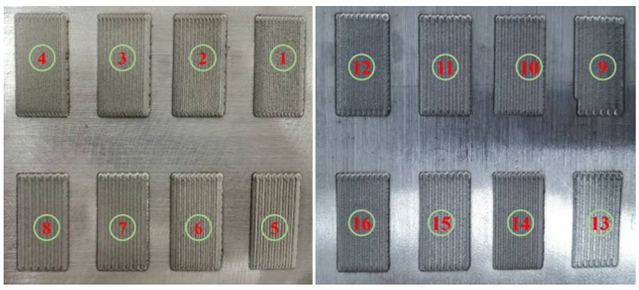

Fig.4 16 sets of parameters for single-layer cladding experiments

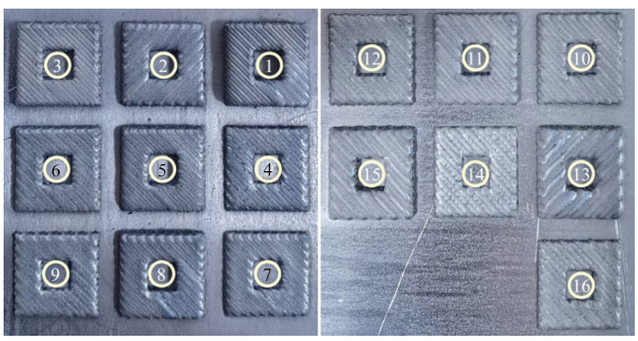

Fig.5 16 sets of parameters for multi-layer cladding experiments

characterize the height error. In principle, this method is also applicable to greater printing thicknesses. Table 5 lists the measurement results for the two response metrics of all specimens.

The point cloud model on top layer of printed part was extracted, and the plane fitting was performed. As shown in Fig.6, the distance from the plane to the substrate is calculated as the actual printing height; subtracting this value from the theoretical height gets the height error. The distance from each point in the top layer point cloud to the fitted plane is calculated, and the average of these distances is taken as the surface roughness of the printed part. During experimental measurements, high-precision measuring equipment was used to ensure the accuracy of the measured data. The possible error range during roughness characterization is attributed to the measurement error of the equipment, which is less than 0.01 mm.

3.2 Calculation of SNR for each response and Taguchi analysis

SNR is introduced as an evaluation index. According to specific requirements, SNR characteristics are divided into three types: larger, smaller, and nominal values, corresponding to the target values of maximizing, minimizing, and reaching or approaching The quality response, respectively. The calculation formulas for these three types are given in Eq.(2–4).

$$\mathrm{SNR} = -10\lg\left(\frac{1}{n}\sum_{i=1}^{n}\frac{1}{y_i^2}\right) \tag{2}$$

$$\mathrm{SNR} = -10\lg\left(\frac{1}{n}\sum_{i=1}^{n}y_i^2\right) \tag{3}$$

$$\mathrm{SNR} = -10\lg\left[\frac{1}{n}\sum_{i=1}^{n}\left(y_i - m\right)^2\right] \tag{4}$$

where SNR is the quality characteristic, n is the number of experiments, m is the experimental target value, and y_i is the experimentally measured data. For the two responses, namely the ΔH and R_a, the goal is to minimize them. Thus, Eq.(3) is employed to calculate SNRs of these two responses. Table 6 lists SNRs values corresponding to each group of experiments.

The mean SNR values for each level are calculated using Eq. (5) to assess the effect of different factor levels on the surface properties of the blade. For a given factor, the factor level yielding the highest mean SNR is considered the optimal level.

$$R_{xi} = \frac{1}{k}\sum_{i=1}^{k}\left(\mathrm{SNR}_i\right) \tag{5}$$

where R_{xi} is the mean value of the SNR corresponding to each factor level, SNR_i is the SNR containing the associated level, and k is the number of experiments.

Extreme deviation is the difference between the highest and lowest average response values of SNR of the factor level. It quantifies the relative impact of different factor levels on experimental outcomes. The larger the extreme deviation, the more significant the influence of that factor. Table 7 shows average SNR value responses of each level for various aspects. Fig. 7 illustrates the trends of SNR for each factor along with the two corresponding responses ΔH and R_a. The SNR analysis reveals that the optimal parameters for minimizing ΔH and R_a are LP1PR1SD3SS4 and LP2PR1SD4SS3, respectively.

According to the SNR ranking analysis, the influence of each process parameter on ΔH of the top layer follows the order: SS>PR>LP>SD. Among these, SS exerts the most significant influence on the cladding layer height. If SS is too slow, the prolonged residence of the laser head in the molten pool leads to an increased heat transfer to either the substrate or the preceding cladding layer, resulting in a progressively higher cladding layer height that surpasses its theoretical value. Conversely, if SS is excessively high, the nozzle injects a reduced amount of metal powder into the molten pool, diminishing the heat transferred to the powder. As a result, the cladding layer height is less than its theoretical value. Therefore, selecting an appropriate SS is crucial for minimizing height errors and improving the quality of printed part.

According to the SNR ranking analysis, the influence of

Table 4 H_1 of cladding layer corresponding to different parameter combinations (mm)

No.	1#	2#	3#	4#	5#	6#	7#	8#	9#	10#	11#	12#	13#	14#	15#	16#
H_1	0.97	0.71	0.82	1.22	1.48	1.32	0.38	0.73	0.39	0.57	0.70	0.61	0.35	0.50	0.45	0.18

Table 5 Measurement results of ΔH and R_a for multi-layer cladding (mm)

No.	ΔH	R_a
1#	2.3442	0.3145
2#	1.0478	0.2003
3#	0.8859	0.1395
4#	3.7846	0.1372
5#	3.4965	0.2191
6#	3.5757	0.1538
7#	1.1789	0.1130
8#	0.5584	0.2102
9#	0.9551	0.0825
10#	1.4096	0.1104
11#	1.4056	0.1369
12#	0.8691	0.1128
13#	2.8770	0.1309
14#	0.0343	0.0974
15#	2.7508	0.1331
16#	1.8251	0.0850

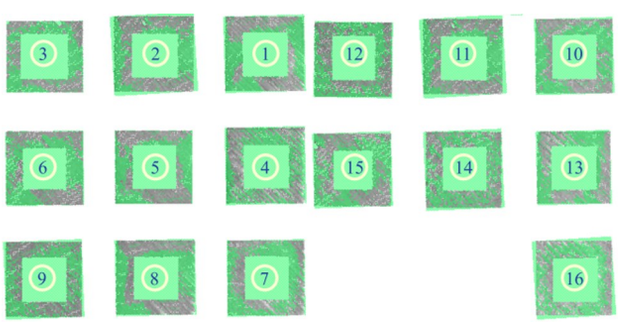

Fig.6 Results of the top layer plane fitting of the printed part

Table 6 SNR of response targets (mm)

No.	ΔH	R_a
1#	−7.400	10.046
2#	−0.406	13.964
3#	1.052	17.110
4#	−11.560	17.252
5#	−10.873	13.187
6#	−11.067	16.261
7#	−1.430	18.938
8#	5.061	13.549
9#	0.440	21.670
10#	−2.982	19.138
11#	−2.957	17.271
12#	1.219	18.952
13#	−9.179	17.660
14#	29.294	20.227
15#	−8.789	17.517
16#	−5.226	21.414

each process parameter on R_a of the top layer follows the order: SD>PR>SS>LP. The roughness of the top surface is mainly affected by the overlap ratio, which is characterized by selected SD in this research. When SD is excessively small, the overlapping area between adjacent cladding layers increases. This may cause excessive material accumulation in a specific area, resulting in protrusions or waviness on the surface and thus increasing the surface roughness. In addition, the heat is concentrated in the overlapping area, which may cause thermal deformation or burning of the cladding material. These phenomena may induce microcracks or defects, further increasing the surface roughness. When SD is excessively large, as the cladding material fails to fully cover the area, insufficient overlap between cladding layers can lead to incomplete local fusion, forming weak zones and an uneven surface, thereby increasing roughness. Moreover, insufficient overlap may diminish the bonding strength between cladding layers, making them prone to peeling or flaking, and thus affecting the overall surface flatness. This is consistent with the conclusions of Ref.[36]. Thus, choosing a suitable SD and corresponding overlap ratio is critical for smoothing surface irregularities of the workpiece and significantly reducing its roughness.

3.3 Multi-objective optimization by grey relational analysis

The Taguchi method is a single-objective response optimization method, while this research aims to optimize two objectives simultaneously. Therefore, the grey relational theory is introduced for multi-objective optimization to determine the optimal laser cladding parameters. The grey relational theory effectively integrates multiple targets into a single objective by converting individual responses into GRG[37].

Grey relational analysis requires a series of calculations[38]. The first step is data normalization. Since the numerical range and unit of each response are different, normalization is necessary. Eq. (6) is used for this normalization, scaling the data to the range between 0 and 1, and its scale remains unchanged. The normalized results are shown in Table 8.

$$X_i(k)=\frac{Y_i(k)-\min\left[Y_i(k)\right]}{\max\left[Y_i(k)\right]-\min\left[Y_i(k)\right]} \tag{6}$$

where $[Y_i(k)]$ is the SNR for the response k (k=1, 2) of experiment i (i=1, 2, ..., 16); max $[Y_i(k)]$ and min $[Y_i(k)]$ are the maximum and minimum values of the response k among all 16 experiments, respectively; $X_i(k)$ is the normalized value of the experiment i and response k.

Then, the grey relational coefficient (GRC) is calculated by Eq.(7)[38].

$$\mathrm{GRC}_i(k)=\frac{\min_i\left|x_i^0-X_i(k)\right|+\xi\max_i\left|x_i^0-X_i(k)\right|}{\left|x_i^0-X_i(k)\right|+\xi\max_i\left|x_i^0-X_i(k)\right|} \tag{7}$$

where $\mathrm{GRC}_i(k)$ is the GRC for the response k (k=1, 2) of experiment i (i=1, 2, ..., 16); x_i^0 is the ideal value of experiment i (i=1, 2, ..., 16) and x_i^0=1 in this work; ξ is the distinguishing coefficient over the range of $0<\xi<1$. In this study, ξ is set to 0.5 by comprehensively considering the

Table 7 Responses of SNR for ΔH and R_a (mm)

Level	ΔH				R_a			
	LP	PR	SD	SS	LP	PR	SD	SS
1	−3.66	4.17	−3.66	−4.15	18.35	19.52	13.93	15.83
2	3.01	0.16	−5.49	−7.50	16.37	16.97	16.15	16.73
3	−3.40	−8.52	−1.08	8.11	17.39	16.56	19.26	17.51
4	−4.66	−4.52	1.53	−5.17	16.43	15.49	19.20	18.47
Delta	7.67	12.70	7.02	15.61	1.97	4.04	5.33	2.64
Rank	3	2	4	1	4	2	1	3

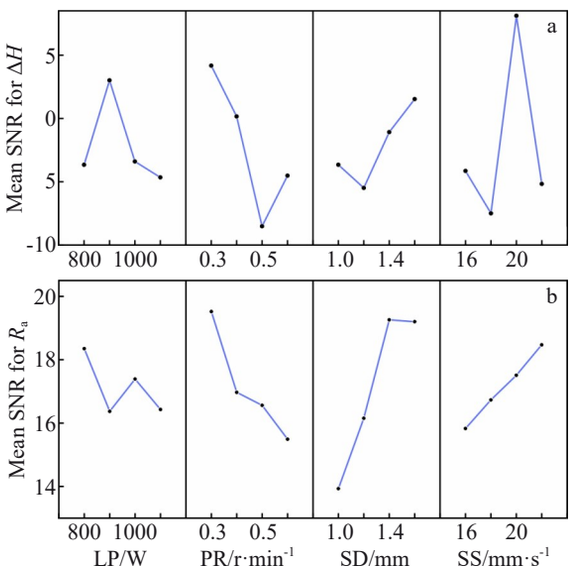

Fig.7 Main effect plots for the SNR analysis of responses: (a) ΔH and (b) R_a

Table 8 Normalized SNR value of response targets (mm)

No.	ΔH	R_a
1#	0.102	0.000
2#	0.273	0.337
3#	0.309	0.608
4#	0.000	0.620
5#	0.017	0.270
6#	0.012	0.535
7#	0.248	0.761
8#	0.407	0.301
9#	0.293	1.000
10#	0.210	0.782
11#	0.211	0.622
12#	0.313	0.766
13#	0.058	0.655
14#	1.000	0.876
15#	0.068	0.643
16#	0.155	0.978

analytic effect and result stability[16]. GRC characterizes the relationship between the actual normalized SNR values and the ideal values, where the ideal values are uniformly set to 1000. Finally, the integrated GRG calculation is achieved using Eq.(8)[38].

$$\mathrm{GRG}_i = \frac{1}{n}\sum_{k=1}^{n}\mathrm{GRC}_i(k) \tag{8}$$

where GRG_i is the GRG of experiment i (i=1, 2, ..., 16), n is the number of the responses, and n=2 in this work. Eq.(8) can equally weigh the importance of ΔH and R_a.

GRC and correlation levels for each process parameter are calculated, as shown in Table 9. To obtain a parameter combination that ensures good printing quality, the Taguchi method is integrated into the grey relational analysis. Fig.8 shows the main effect plot of GRG. According to the analysis, the optimal process parameter combination is LP1PR1SD3SS3; LP is 800 W, PR is 0.3 r/min, SD is 1.6 mm, and SS is 20 mm/s.

In addition, Table 10 shows the importance ranking of factors with respect to the GRG, which follows the order: SD>PR>SS>LP. SD plays a leading role in influencing both the height error and roughness.

3.4 Experimental verification of optimal parameters

An additional verification experiment is necessary since the

Table 9 Grey relational analysis data for responses

No.	GRC		GRG	
	ΔH	R_a	Value	Rank
1#	0.358	0.333	0.345	16
2#	0.408	0.430	0.419	14
3#	0.420	0.560	0.490	7
4#	0.333	0.568	0.451	11
5#	0.337	0.407	0.372	15
6#	0.336	0.518	0.427	13
7#	0.399	0.680	0.540	6
8#	0.457	0.417	0.437	12
9#	0.414	1.000	0.707	2
10#	0.388	0.679	0.542	5
11#	0.388	0.569	0.478	8
12#	0.421	0.681	0.551	4
13#	0.347	0.592	0.469	9
14#	1.000	0.801	0.814	1
15#	0.349	0.583	0.466	10
16#	0.372	0.958	0.665	3

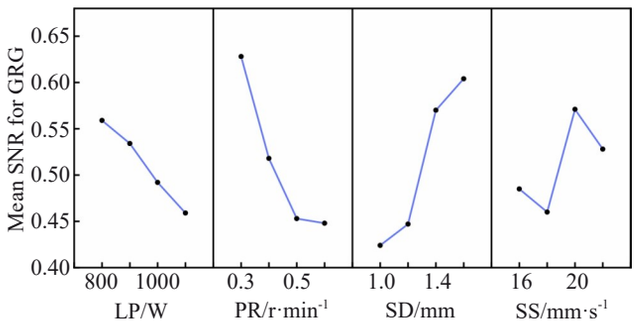

Fig.8 Main effect plots for the SNR analysis of GRG

Table 10 Responses for SNR of GRG

Level	LP	PR	SD	SS
1	0.559	0.628	0.424	0.485
2	0.534	0.518	0.447	0.460
3	0.492	0.453	0.570	0.571
4	0.459	0.448	0.604	0.528
Delta	1.434	2.846	2.958	1.707
Rank	4	2	1	3

optimal parameter combination is not involved in the $L_{16}(4^4)$ orthogonal array. Eq.(9)[38] can predict the GRG.

$$GRG_p = GRG_m + \sum_{j=1}^{n}\left(GRG_j - GRG_m\right) \quad (9)$$

where GRG_m is the mean value of total GRG; n is the number of process parameter and n=4 in this work; GRG_j is the mean value of all GRG for processing parameter j (j =1, 2, 3, 4) at its optimal level; GRG_p is the predicted GRG at the selected level.

With the optimal process parameters, the GRG_p is 0.828. Comparing the results of the single-target response for ΔH and R_a with the grey relational analysis results, it can be seen that the predicted results of GRG_{Prc} and the experimentally calculated GRG_{Exp} exhibit consistent trends in magnitude, as shown in Table 11. This further confirms that the parameters obtained by the multi-target grey relational analysis are optimal.

3.5 Multi-objective prediction based on GB-BP network

Due to the complexity of the metal LDED process and the inherent variability in product requirements, it is not advisable to conduct individual experiments. Instead, a mapping relationship between process parameter combinations and responses should be established based on a few samples. Artificial neural network (ANN) is a computational model miming biological neural networks[39]. Its architecture typically contains an input layer responsible for receiving input data, multiple hidden layers that process and extract features from the input data, and an output layer that generates the final result. The BP network is the most widely used ANN model[40]. It employs BP algorithm to optimize the weights and biases of network, thereby improving the accuracy of model. The structural diagram of the BP network is shown in Fig. 9. This method establishes the correlation between input process parameters (LD, PR, SD, and SS) and output parameters (R_a and ΔH).

The appropriate number of neurons enhances the prediction accuracy of network. Bayesian optimization (BO) is employed to determine the optimal configuration, including hidden layers, neurons, and network learning rate[41]. BO constructs a Gaussian process probability model to represent the possible distribution of the objective function.

The model is updated by randomly selecting a set of points for evaluation. Therefore, new evaluation points are identified and added to the model for iterative refinement. This process is repeated until either the maximum number of iterations is reached or a predetermined level of accuracy is converged upon. The parameters of the selected BP network are shown in Table 12. The initial 14 datasets from Table 5 serve as the training set, and the last two datasets constitute the testing set. The root mean square error (RMSE) is used to evaluate the network performance, as shown in Eq.(10).

Table 11 Comparison of single-target response and multi-target response results

Parameter	ΔH	R_a	ΔH+R_a
LP/W	800	900	800
PR/r·min^{-1}	0.3	0.3	0.3
SD/mm	1.4	1.6	1.6
SS/mm·s^{-1}	22	20	20
GRG_{Exp}	0.719	0.721	0.807
GRG_{Prc}	0.751	0.804	0.828

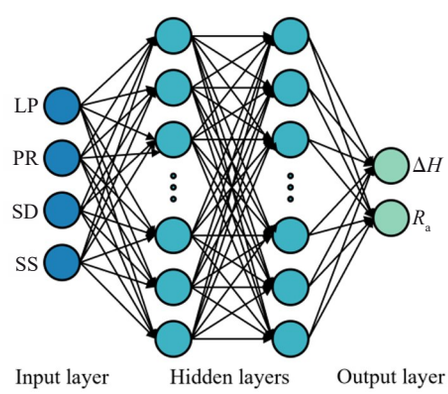

Fig.9 Topology diagram of BP network

Table 12 Parameters of BP network

Parameter	Value
Activation function	Sigmoid
Optimizer	Adam
Epoch	600
Learning rate	0.027
Number of hidden layers	2
Number of nodes in the first hidden layer	10
Number of nodes in the second hidden layer	6

$$\mathrm{RMSE} = \sqrt{\frac{1}{n}\sum_{i=1}^{n}\left(Y_i - \hat{Y}_i\right)^2} \quad (10)$$

where n is the number of samples, Y_i is the ground truth for each data set, and $\hat{Y}_i$ is the predicted output of the network.

Fig. 10 illustrates the loss function curve. The relative prediction errors for ΔH and R_a are calculated to be 51% and 21%, respectively, as shown in Table 13. The relative error for ΔH is higher than 50%, indicating that its prediction performance is not ideal. The BP network is likely to get trapped under the local optima, resulting in unsatisfactory training effects. In addition, overfitting will occur when the training data are insufficient, decreasing the generalization ability of model for new data.

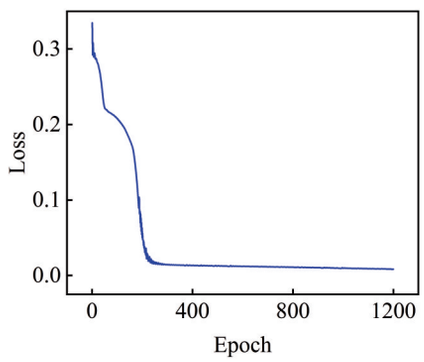

Fig.10 Loss function curve of the BP network

Table 13 Comparison of relative prediction errors between BP and GB-BP networks (%)

Prediction	ΔH		R_a	
	BP	GB-BP	BP	GB-BP
Relative error	51	29	21	6

GA mimics the natural process of biological evolution, employing selection, crossover, and mutation operations to search for optimal solutions. It initializes a population to explore the solution space, enabling it to handle multiple problems and optimize multiple parameters simultaneously[42]. Consequently, GA was introduced to replace the BP process in the BP network, enabling accurate prediction of multiple responses[43]. The algorithm flowchart is shown in Fig.11. The weights and biases of the BP network are encoded as chromosomes, with their values constrained within the range [−1, 1]. The fitness function is the mean square error (MSE), as denoted by Eq. (11). The GB-BP parameters were determined through experiments, as shown in Table 14.

$$\mathrm{MSE} = \frac{1}{n}\sum_{i=1}^{n}\left(Y_i - \hat{Y}_i\right)^2 \quad (11)$$

where n is the number of test sets, Y_i is the ground truth, and $\hat{Y}_i$ is the network predict value.

Similar to the BP network, the first 14 datasets from Table 5 were selected as the training set, and the last two datasets

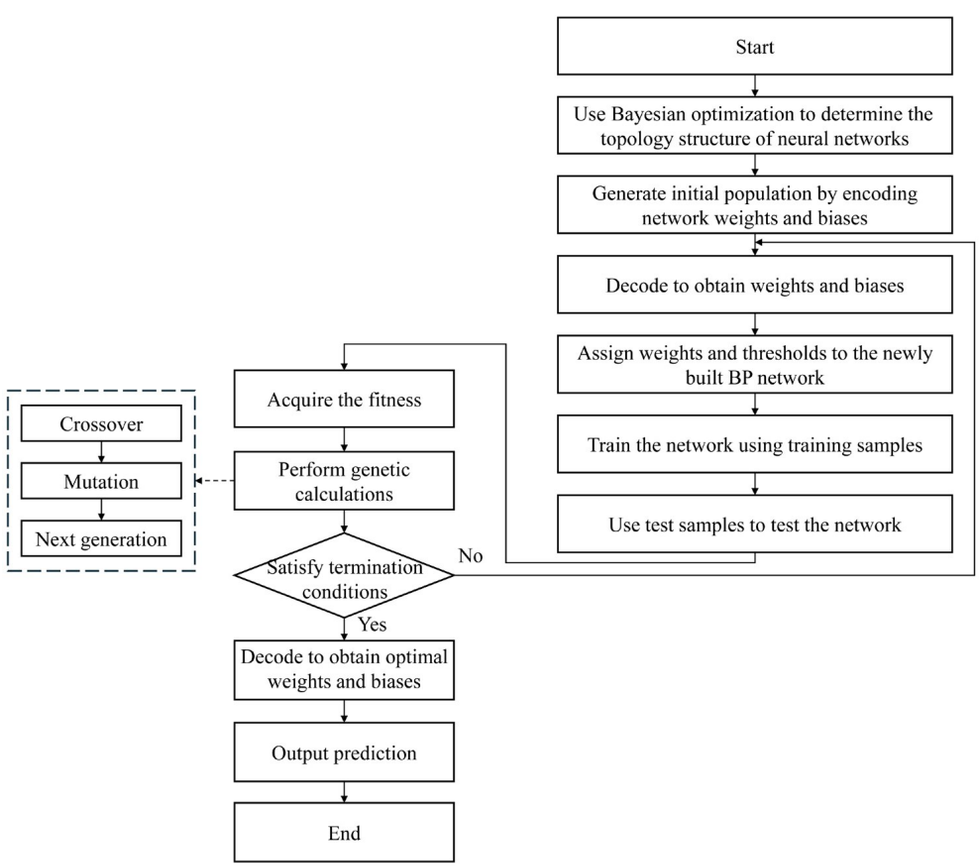

Fig.11 Flow chart of GB-BP network

Table 14 Parameters of GB-BP network

Parameter	Value
Coding method	Real number coding
Max iteration	6000
Population size	80
Elite ratio	0.06
Parents portion	0.5
Crossover probability	0.54
Mutation probability	0.01
Crossover type	Uniform
Number of nodes in the first hidden layer	10
Number of nodes in the second hidden layer	6

serve as the testing set. Fig. 12 illustrates the loss function curve, which appears much smoother compared to that of the BP network. This is because, after the introduction of GA, the BP network can adjust weights according to gradients derived from GA optimization, enabling the fine-tuning of the model and avoiding loss fluctuations caused by overfitting. Additionally, GA eliminates reliance on a fixed learning rate. Instead, it determines the direction and amplitude of weight updates through evolutionary processes, resulting in a more stable training process. Fig. 13c – 13d show the prediction results of the GB-BP network. The relative prediction errors for ΔH and R_a are calculated to be 29% and 6%, respectively, as shown in Table 13. These results show that the prediction error for ΔH is larger than that for R_a. The main reason is that, compared with R_a, the response of ΔH has a weaker correlation with several process parameters mentioned in this research. In addition, the predictions of the network are based on a model trained with a small sample size. If the number of training samples is increased, the prediction accuracy will be improved to a certain extent.

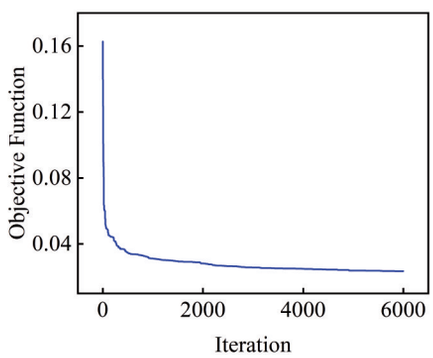

Fig.12 Objective function curve of GB-BP network

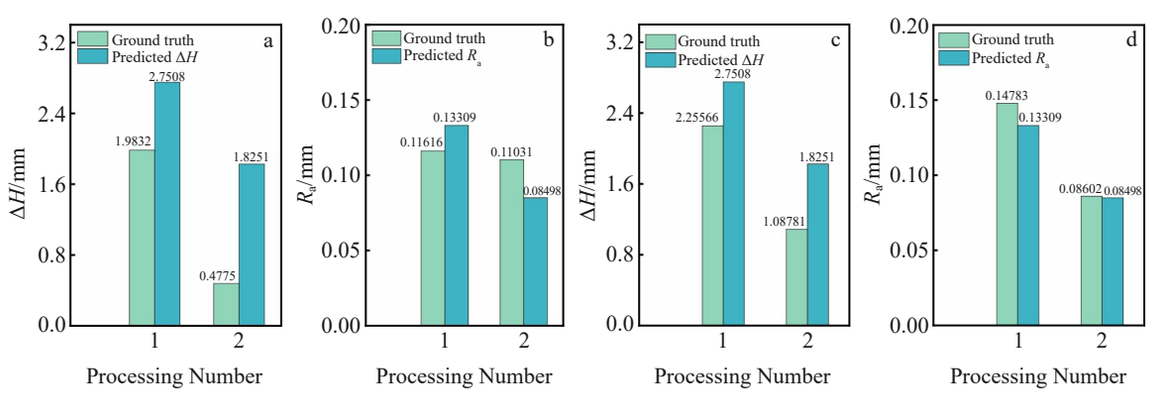

Fig.13 Comparison between results predicted by BP (a–b) and GB-BP (c–d) networks: (a, c) ΔH and (b, d) R_a

It is evident that compared to that of the BP network predictions, the relative error of the GB-BP network predictions is significantly reduced, and the prediction accuracy is greatly improved. Compared with the traditional BP network, the GB-BP network has improved prediction accuracy of ΔH and R_a by 43.14% and 71.43%, respectively.

The k-fold cross-validation method was used to verify the generalization ability of the GB-BP network[44]. The dataset was divided into eight folds, each containing two data groups. In each iteration, 7 folds (14 datasets) were used for training, and one fold (2 datasets) was used for verification. This process was repeated 8 times to complete all training and validation cycles, with the results shown in Table 15. The results show that the average relative error of the GB-BP network in predicting ΔH is 42%, and that for R_a is 19%, which are much smaller than the prediction errors of the BP

Table 15 Cross-validation results of GB-BP network (%)

No.	Relative error	
	ΔH	R_a
1#	40	19
2#	37	19
3#	26	19
4#	33	29
5#	44	18
6#	64	13
7#	38	18
8#	52	18

network. It is proved that the GB-BP network can accurately predict multiple responses and has strong generalization ability.

4 Conclusions

1) A visual inspection system was constructed to characterize the surface morphology quality of the printed parts. Through collection and analysis of data, the height error and surface roughness between the point cloud model of the printed part and the theoretical model are calculated, serving as performance parameters for evaluation.

2) Through Taguchi experiments and SNR analysis, the influence order of process parameters on the individual response of ΔH is SS>PR>LP>SD. For the individual response of R_a, the influence order is SD>PR>SS>LP. Using the grey relational analysis method to evaluate the multi-objective response, the influence order of process parameters is SD>PR>SS>LP. The optimal parameter combination is determined to be LP1PR1SD3SS3, with specific values: LP of 800 W, PR of 1.6 r/min, SD of 1.6 mm, and SS of 20 mm/s.

3) Considering the multifactorial characteristics of the metal powder LDED process, a GB-BP network is designed to predict the ΔH and R_a of printed parts, aiming to improve manufacturing efficiency. The BO algorithm is used to determine the optimal number of hidden layers and nodes for the BP network, while GA replaces the BP process to improve its performance. Experimental verification shows that the GB-BP network significantly improves prediction accuracy compared with the traditional BP network, with the prediction accuracy of ΔH and R_a increasing by 43.14% and 71.43%, respectively.

4) The future research will focus on expanding the dataset and refining the network, aiming to improve the accuracy of multi-target response predictions for multi-layer and multi-pass metal printed parts.

References

1 Guo N, Leu M C. *Frontiers of Mechanical Engineering*[J], 2013, 8: 215

2 Dawood A, Marti B M, Sauret-Jackson V *et al*. *British Dental Journal*[J], 2015, 219(11): 521

3 Gradl P R, Protz C S, Wammen T. *AIAA Propulsion and Energy 2019 Forum*[C]. Reston: Aerospace Research Central, 2019: 4362

4 Fan Yongxia, Lin Yan, Ao Qingbo *et al*. *Rare Metal Materials and Engineering*[J], 2023, 52(10): 3630 (in Chinese)

5 Zhang J, Zhang Q L, Chen Z J *et al*. *Journal of Laser Applications*[J], 2019, 31(3): 032016

6 Kistler N A, Nassar A R, Reutzel E W *et al*. *Journal of Laser Applications*[J], 2017, 29(2): 022005

7 Hussain M, Kumar V, Mandal V *et al*. *Materials and Manufacturing Processes*[J], 2017, 32(14): 1667

8 Mondal S, Bandyopadhyay A, Pal P K. *The International Journal of Advanced Manufacturing Technology*[J], 2014, 70: 2151

9 Lin J L, Lin C L. *International Journal of Machine Tools and Manufacture*[J], 2002, 42(2): 237

10 Tsai M J, Li C H. *Optics & Laser Technology*[J], 2009, 41(8): 914

11 Fu C Y, Zheng J S, Zhao J M *et al*. *Corrosion Science*[J], 2001, 43(5): 881

12 Ge W G, Guo C, Lin F *et al*. *Rare Metal Materials and Engineering*[J], 2015, 44(11): 2623

13 Javid Y. *CIRP Journal of Manufacturing Science and Technology*[J], 2020, 31: 406

14 Fatoba O S, Akinlabi E T, Akinlabi S A *et al*. *Materials Today: Proceedings*[J], 2018, 5(9): 19181

15 Marzban J, Ghaseminejad P, Ahmadzadeh M H *et al*. *The International Journal of Advanced Manufacturing Technology*[J], 2015, 76: 1163

16 Deng D W, Li T S, Huang Z Y *et al*. *Optics & Laser Technology*[J], 2022, 153: 108259

17 Mondal S, Paul C P, Kukreja L M *et al*. *The International Journal of Advanced Manufacturing Technology*[J], 2013, 66: 91

18 Quazi M M, Fazal M A, Haseeb A *et al*. *Tribology Transactions*[J], 2017, 60(2): 249

19 Yu T B, Yang L, Zhao Y *et al*. *Optics & Laser Technology*[J], 2018, 108: 321

20 Lian G F, Zhao C M, Zhang Y *et al*. *Applied Sciences*[J], 2020, 10(9): 3167

21 Lee E M, Shin G Y, Yoon H S *et al*. *Journal of Mechanical Science and Technology*[J], 2017, 31: 3411

22 Alam M K, Urbanic R J, Nazemi N *et al*. *The International Journal of Advanced Manufacturing Technology*[J], 2018, 94: 397

23 Bhardwaj T, Shukla M, Paul C P *et al*. *Journal of Alloys and Compounds*[J], 2019, 787: 1238

24 Yin F, Mao H J, Hua L. *Materials & Design*[J], 2011, 32(6): 3457

25 Mohajernia B, Mirazimzadeh S E, Pasha A *et al*. *The International Journal of Advanced Manufacturing Technology*[J], 2022, 118: 1

26 Li Y T, Wang K M, Fu H G *et al*. *Coatings*[J], 2021, 11(11): 1402

27 Lestan Z, Klancnik S, Balic J *et al*. *Materials and Manufacturing Processes*[J], 2015, 30(4): 458

28 Ilanlou M, Razavi R S, Nourollahi A *et al*. *Optics & Laser Technology*[J], 2022, 156: 108507

29 Yang Y W, Tian Z J, Pan H *et al*. *Transactions of the China Welding Institution*[J], 2013(11): 78

30 Liu H M, Qin X P, Huang S *et al*. *International Journal of Precision Engineering and Manufacturing*[J], 2018, 19: 1061

31 Yu J T, Sun W M, Huang H B *et al*. *Coatings*[J], 2019, 9(11): 728

32 Deng Z X, Chen T, Wang H J *et al*. *Applied Sciences*[J], 2020, 10(18): 6331

33 Wang S H, Zhu L D, Fuh J Y H *et al*. *Optics and Lasers in*

Engineering[J], 2020, 127: 105950
34 Kumar P, Jain N K, Sawant M S. *Journal of Materials Research and Technology*[J], 2022, 17: 95
35 Ahmed N, Barsoum I, Haidemenopoulos G *et al*. *Journal of Manufacturing Processes*[J], 2022, 75: 415
36 Zhang Y, Xu Y, Sun Y *et al*. *Surface Topography: Metrology and Properties*[J], 2022, 10(4): 044007
37 Lian G F, Zhang H, Zhang Y *et al*. *Coatings*[J], 2019, 9(6): 356
38 Lian G F, Xiao S H, Zhang Y *et al*. *The International Journal of Advanced Manufacturing Technology*[J], 2021, 112: 1449
39 Okuyucu H, Kurt A, Arcaklioglu E. *Materials & Design*[J], 2007, 28(1): 78
40 Li Y P, Liu Y Y, Luo S H *et al*. *Journal of Materials Research and Technology*[J], 2020, 9(6): 14467
41 Snoek J, Larochelle H, Adams R P. *Advances in Neural Information Processing Systems*[J], 2012, 25: 636
42 Ding S F, Su C Y, Yu J Z. *Artificial Intelligence Review*[J], 2011, 36: 153
43 Li H L, Wu D B, Wang H. *Measurement*[J], 2025, 242: 115732
44 Wong T T. *Pattern Recognition*[J], 2015, 48(9): 2839

多层多道次LDED工艺参数智能决策与多目标预测

李亚冠[1,2]，聂振国[2,3,4]，李荟林[2]，王　涛[1]，黄庆学[1]
(1. 太原理工大学 机械工程学院，山西 太原 030024)
(2. 清华大学 机械工程系，北京 100084)
(3. 清华大学 先进装备摩擦学国家重点实验室，北京 100084)
(4. 清华大学 精密超精密制造装备及控制北京市重点实验室，北京 100084)

摘　要：表征多层多道次激光金属打印件形貌质量的主要参数是表面粗糙度和实际打印高度与理论模型高度之间的误差。采用田口法建立工艺参数组合与金属打印形貌质量（高度误差和粗糙度）多目标表征之间的关联性。先通过信噪比和灰色关联分析法预测多层多道次打印的最优参数组合为：激光功率800 W、送粉速率0.3 r/min、步距1.6 mm、扫描速度20 mm/s；随后构建遗传贝叶斯-反向传播（GB-BP）网络对多目标响应进行预测。与传统反向传播网络相比，GB-BP网络对高度误差和表面粗糙度的预测精度分别提高了43.14%和71.43%。该网络可以准确预测多层多道次激光定向能量沉积金属打印部件的形貌和质量的多目标表征。

关键词：多层多道次激光熔覆；田口法；灰色关联分析；GB-BP网络

作者简介：李亚冠，男，1995年生，博士，太原理工大学机械工程学院，山西 太原 030024，E-mail：liyaguan0014@link.tyut.edu.cn